Proceedings of International Collaboration on Advanced Neutron Sources (ICANS-VII), 1983 September 13-16
Atomic Energy of Canada Limited, Report AECL-8488

THERMOFLUID DYNAMICS IN LIQUID TARGETS

Y. Takeda
Swiss Institute for Nuclear Research
CH-5234 Villigen, Switzerland

1. INTRODUCTION

The design concept for the SINQ target is to use Lead Bismuth Eutectic (LBE) in the liquid phase in a vertical cylindrical container, with the proton beam entering from the bottom. Natural convection of LBE is to be utilized to transport the deposited energy to a heat exchanger at the top. The thermofluid dynamics of this liquid target is one of the important study subjects for a practical design. A program including theoretical studies and experimental work eventually leading to a full scale test with LBE, is in progress.

The thermofluid behaviour of LBE has been calculated and the effects of several parameters studied. The calculated flow patterns show in many cases a single circulation which contains the majority of the LBE in the target. This is considered to be a desirable feature for the operational target and will be referred to as "total circulation". Several power law relationship between thermofluid-dynamical properties and physical conditions of the target system have been obtained, which are helpful for further applications.

Experimentally, the fluid motion of natural convection of water has been visualised with a small scale apparatus and the development of the circulation of liquid and flow patterns investigated. A threshold Grasshof number to reach "total circulation" has been obtained. A large scale experimental setup is now in operation.

2. CALCULATIONS OF THERMOFLUID BEHAVIOUR

Details of the theoretical model and the calculational method have been given in an earlier report[1]. A series of calculations have been performed in order to see the effects of target height, beam power, beam radius and adiabatic side walls. For the adiabatic side walls two sets of calculations were carried out, one with constant height of target and changing the height of the adiabatic wall, the other with constant height of adiabatic wall and changing the target height.

2.1 Target height

Temperature distributions and flow patterns have been calculated for targets of height from 75 cm to 450 cm. Fig. 1 shows these distributions at the stationary state. For all cases the flow patterns show "total circulation" although their centers are displaced vertically.

The time traces of the maximum temperature are shown in Fig. 2. The development of the temperature distribution during the initial transient was discussed in reference 1. The duration of the transient as a function of height (L) is plotted in Fig. 3 and shows a linear relationship; this is expected since the transient time is proportional to L/U and the characteristic thermal velocity U does not depend on the target height. The maximum temperature rise above the initial temperature (taken as the melting point of LBE) for the stationary states is the same for all four cases and about 25° C.

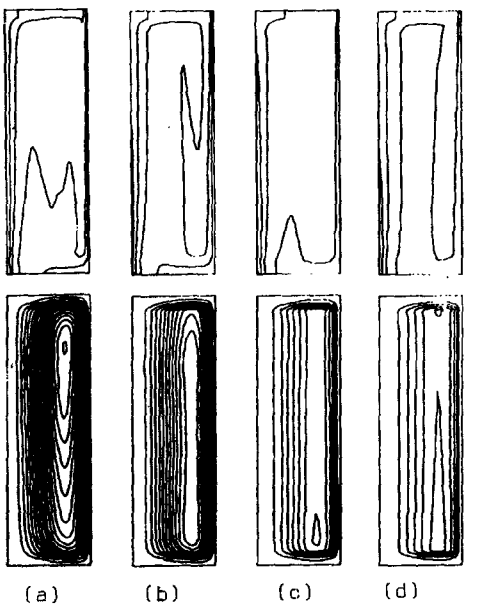

Fig. 1 Distribution of temperature and stream function at stationary state. a) is 75 cm at 25.5 sec, b) 150 cm at 51.0 sec, c) 300 cm at 102.0 sec, and d) 450 cm at 146.8 sec.

Although the development of the flow to "total circulation" during the initial transient is fairly smooth for a target height lower than 300 cm, a multi-cell structure can be seen (Fig. 4) for the 450 cm target. However, this does not persist and is subdued by the stronger "total circulation" once it is fully developed. The temperature distribution is also influenced by this multicell structure, and some distortion of the contour lines can be seen in the upper portion of the target.

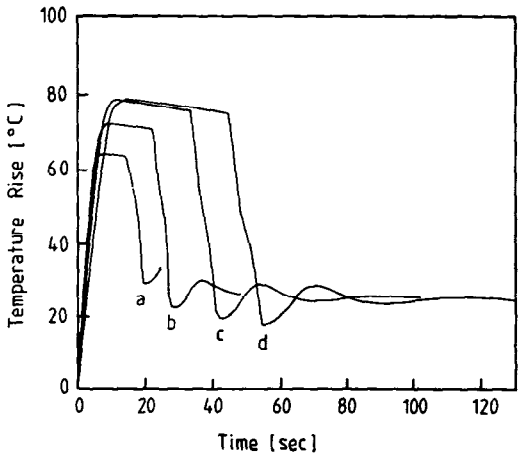

Fig. 2 Time traces of the maximum temperature for target heights; a) 75, b) 150, c) 300 and d) 450 cm.

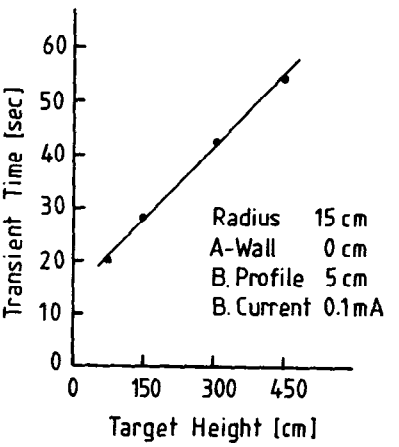

Fig. 3 Transient time versus target height.

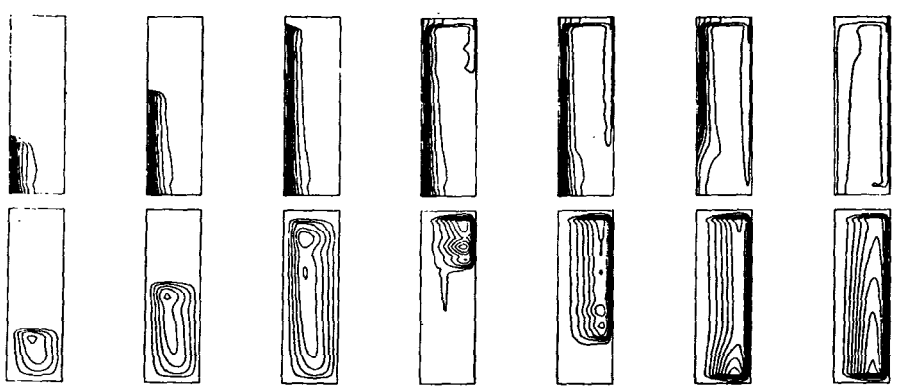

Fig. 4 Time change of the temperature distribution and stream function distribution for a target height of 450 cm. dT is 0.05 (6.25°C) for all and dΨ is 2 for a)-c) and 10 for d)-g).

2.2 Beam power

To see the effect of beam power, calculations with three different beam currents, 0.1, 0.5 and 1 mA (1 mA ≈ 0.6 MW) have been made. The distributions of temperature and stream function are very similar for the three cases and "total circulation" is obtained.

The maximum temperature rise at the stationary state is plotted as a function of beam current in Fig. 5, and shows a simple power-law relationship. The estimate of the exponent is 0.73, which is within 10 % of the value, 2/3 given by a simple one-dimensional analysis[2].

2.3 Beam profile

Three calculations were performed with beam sizes (values of σ_0 in Eq. 11 of reference 1) of 2.5, 5.0 and 10.0 cm. The center of the circulation shortly after start of heating moves to larger radii as the beam size is increased (Fig. 6), that is, the broader beam generates a rising column with a larger radius about the center line. However, at the stationary state the centers are situated at the same radial position. Fig. 7 shows the variation of axial velocity at mid-center with beam radius.

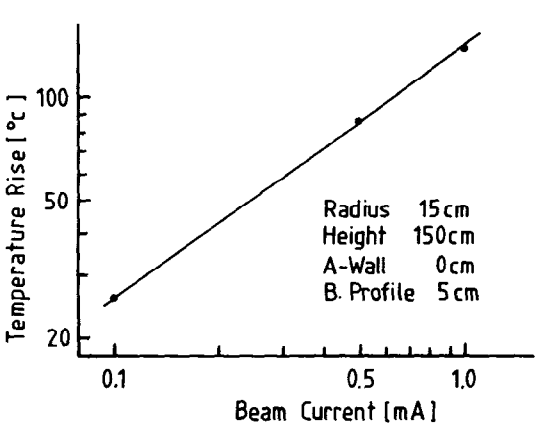

Fig. 5 Power-law relationship for the temperature rise at the stationary state with input beam current.

It shows a fairly good power law relationship to the beam radius R. The estimate of its exponent is -0.6. Simply considered, the convected power is a product of velocity v and temperature rise T and is proportional to the power deposition density q. Since $T \propto q^{2/3}$ (from the previous section) then $v \propto q^{1/3}$ and as $q \propto R^{-2}$ the velocity should be $\propto R^{-2/3}$. The estimate for the exponent is within 10 % of this value, and this relationship is consistent with that for Fig. 5. The temperature-rise at the stationary state as a function of beam profile is shown in Fig. 8. It is lower for the cases with broader beam as expected from the simple analysis ($\propto R^{-4/3}$).

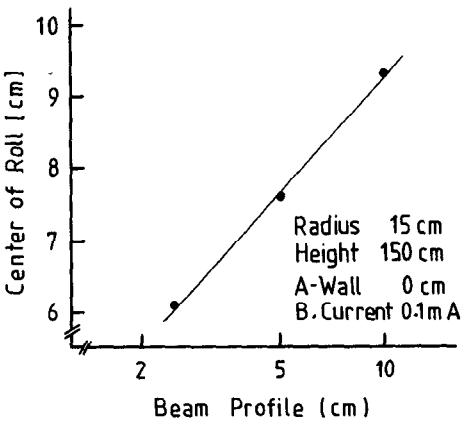

Fig. 6 Positions of the center of circulations at initial stages as a function of beam profile.

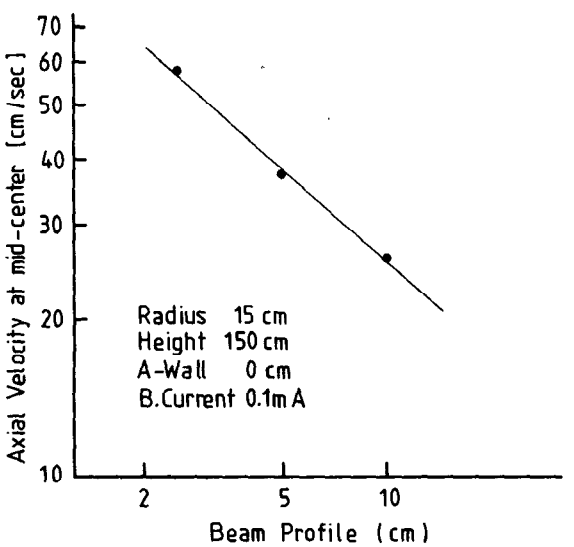

Fig. 7 Axial velocity (v_2) at mid-central position versus beam profile.

2.4 Adiabatic wall with fixed target height

Using a fixed target height of 150 cm, the effects of adiabatic side walls have been studied by calculating systems with their height set to 50, 75 and 100 cm. The adiabatic walls are at the lower end of the target. The calculated flow patterns are very similar to those obtained with a conducting wall, and show "total circulation". The small difference

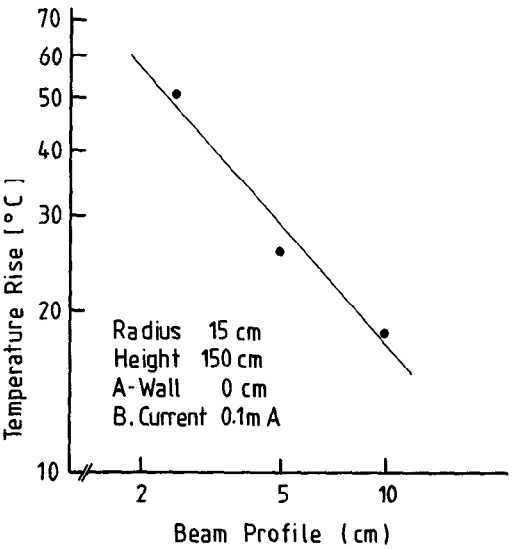

Fig. 8 Temperature rise at the stationary state versus beam profile.

in the velocity distribution is plotted as a function of height in Fig. 9.
With an adiabatic side wall the velocity is increased by about 10 % in the region above the level of the adiabatic wall, but it is only slightly increased elsewhere.

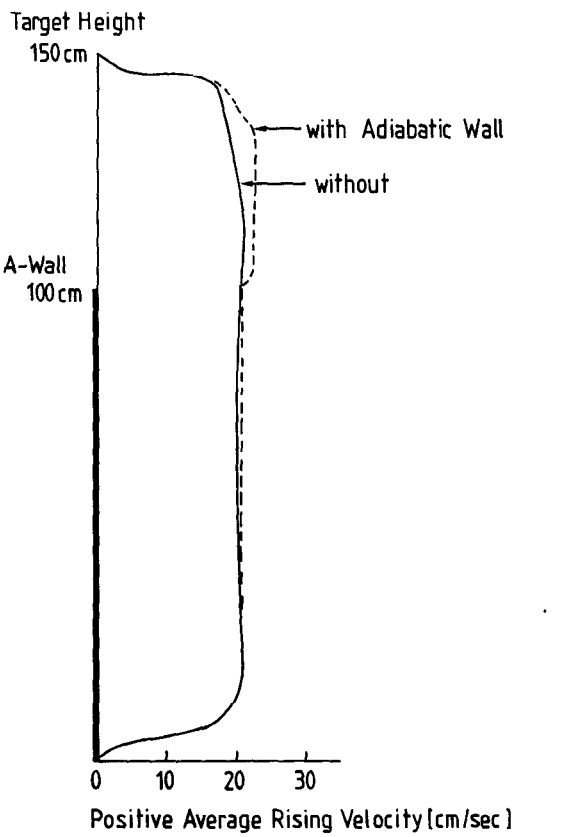

Fig. 9 Comparison of the average positive axial velocity as a function of height for the results with and without adiabatic wall at 51.0 sec.

In the boundary layer near the side wall, there is, as may be expected, a steep temperature gradient toward the conducting surface.

Fig. 10 is the time trace of the maximum temperature. The behaviour during the initial transient is exactly the same for all three cases. This is due to the fact that the temperature of the central portion is not influenced by the conducting wall until "total circulation" is established. Since the smaller cooling area for the higher adiabatic walls results in a higher heat transfer per unit area and hence higher temperature difference, the maximum temperature after the transient naturally becomes higher. For the case of the 100 cm wall the temperature still increases with time.

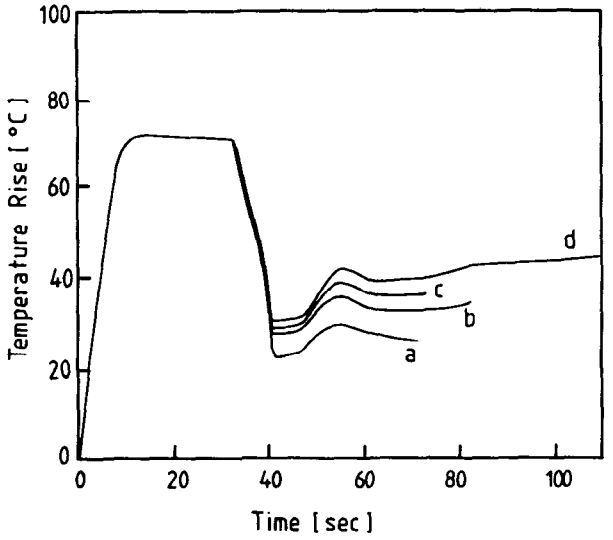

Fig. 10 Time traces of the maximum temperature for various heights of adiabatic side wall. a) is for total conducting wall, b) is 50 cm, c) 75 cm and d) 100 cm.

2.5 Adiabatic side wall with fixed height

Calculations were made for systems with a fixed 100 cm height of adiabatic side wall for five different target heights. The flow patterns show "total circulation" for all cases. However, the temperature distributions become more complicated as the target height is reduced. This is due to the smaller heat transfer area, as discussed in 2.4.

The maximum temperature rise at the stationary state is plotted in Fig. 11 as a function of the target height for cases with and without adiabatic side walls. For a target height larger than 300 cm, the difference between with and without adiabatic wall is only slight.

2.6 Summary

The results of these calculations show that within the parameter value variations studied here, natural convection of target fluid is stable and the temperature distributions are uncomplicated. Power laws for the maximum temperature rise with beam power, beam profile and height of adiabatic walls, are helpful for practical design work.

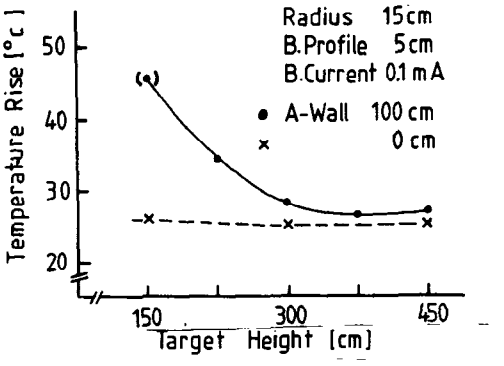

Fig. 11 Temperature rise at the stationary state versus target height with fixed height of adiabatic side wall of 100 cm. The values from the results with total conducting wall are also plotted. As the value for the target height of 150 cm is not at a stationary state, it is plotted in a bracket.

3. EXPERIMENTAL OBSERVATION OF NATURAL CONVECTION IN WATER

As a part of the experimental verification of the calculations, some small scale experiments have been carried out to observe the fluid

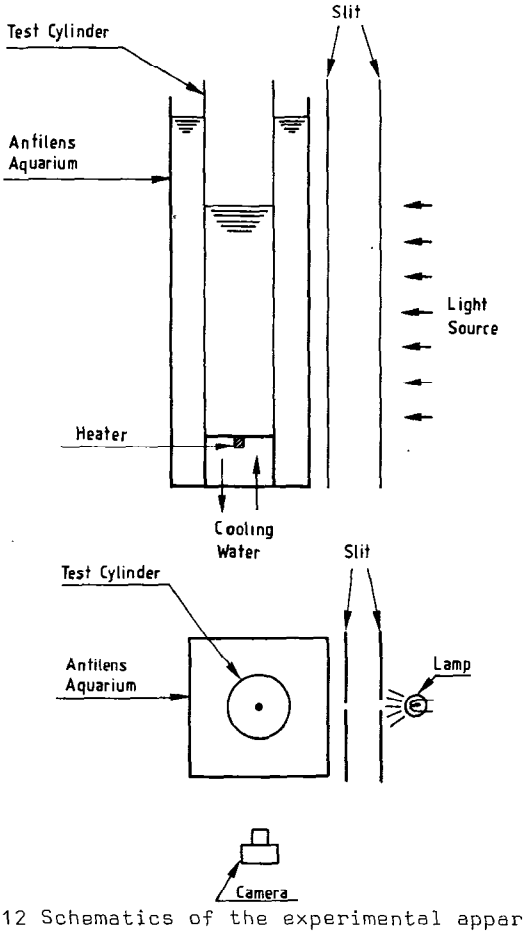

Fig. 12 Schematics of the experimental apparatus arrangement. a) front view, b) top view.

behaviour of natural convection in water. The main interest of this experiment is to study the total fluid motion in a cylinder rather than any local effects like boundary layer flow.

3.1 Apparatus

The apparatus shown in Fig. 12 was used. A glass cylinder of 2.7 cm radius and 55 cm height is set in a square aquarium. The aquarium was used to keep the wall temperature of the cylinder constant and to act as an antilens for taking photographs. The bottom plate is made of Derlin and has a heating area of 9 mm diameter at the center. This plate is water-cooled. The temperature of the heated area was measured by a sheated CA thermocouple at 1.5 mm below the center of the top surface. The wall temperature of the glass cylinder was measured at 10 cm from bottom. The top surface is open and free. The "Aluminium powder method" was used for visualisation of the flow.

3.2 Results

The observed flow motions have been categorised into several patterns, a] partial circulation (only near the heated area), b] "total circulation"(a single roll in a water), c] multi-rolls (vertically several rolls appeared and disappeared) d] swaying core or other three-dimensional motions. The appearance of these flow patterns depends on Gr number and the aspect ratio..For a fixed aspect ratio, only a partial circulation a) is generated at low Gr number, and with increase of Gr, a "total circulation" b] is generated. Photographs of "total circulation" for various water heights are shown in Fig. 13. These stationary state flows could be maintained for several hours. Further increase of Gr leads eventually to flow patterns as in c] or d] Fig. 14 is a map of flow patterns of type a] and b] in a G-γ plane. The definition of Gr is given in the figure, and γ is the aspect ratio defined as L/R. There is a threshold value of Gr for generating "total circulation" which depends on the aspect ratio. As this dependency changes at aspect ratios in the region of 8-10, two straight lines for these threshold values are drawn in the figure. The dependence is larger for smaller aspect ratio (line-1) and vice versa (line-2). Also shown in the figure are two curves derived from the literature. The first is of an empirical critical Gr number in a vertical rectangular box compiled by Ostrach[3], the second, a theoretical critical Gr number in an infinite parallel plate system, derived by Eckert[4].

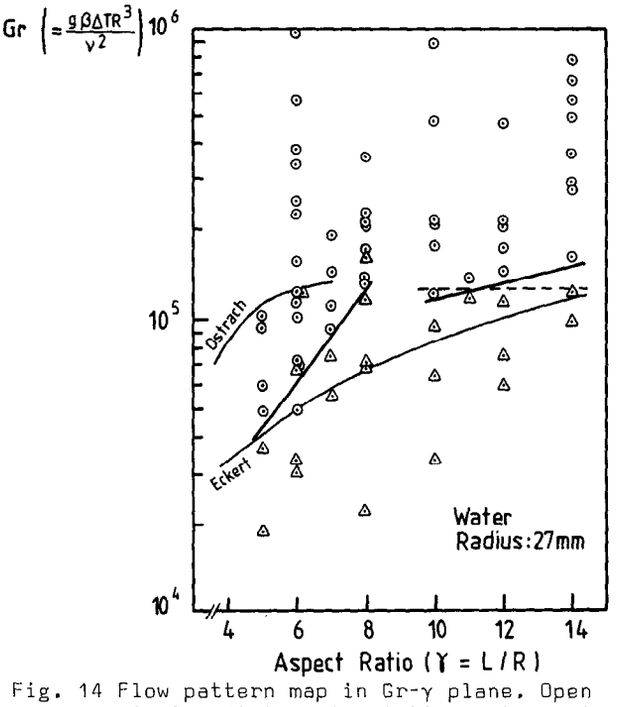

Fig. 14 Flow pattern map in Gr-γ plane. Open circles "total circulation", triangles "partial circulation" (undeveloped flow).

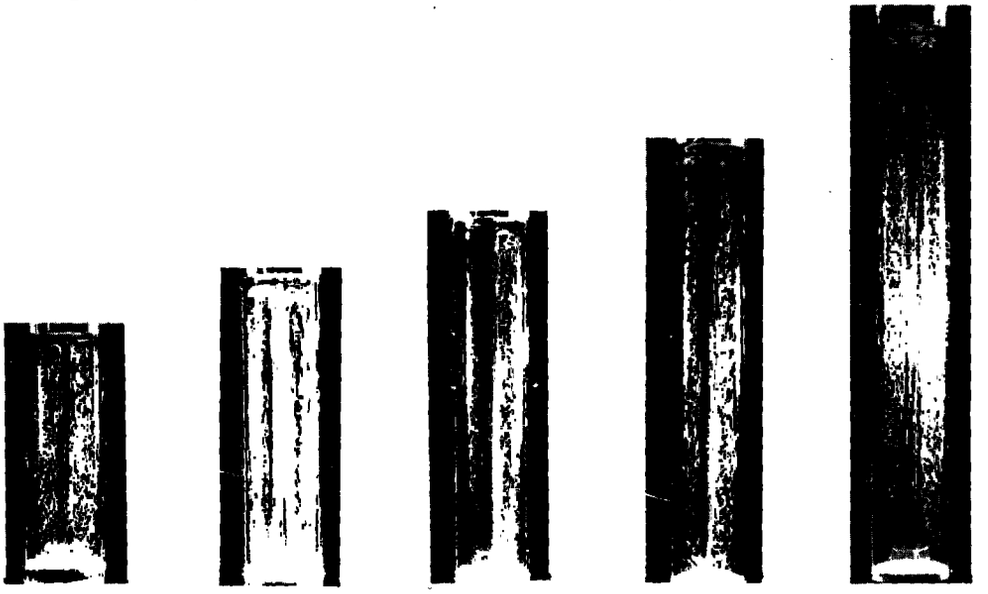

Fig. 13 "Total circulation" for various heights of water.

For both, the temperature difference is applied to two opposite vertical side walls. The gradient of line-1 is close to that of the "Ostrach line" and of line-2 close to that of the "Eckert line". This implies that for an aspect ratio smaller than 8 the effect of the top and bottom surface is large, and for larger aspect ratio than 10 the problem might be treated as a system of infinite height. The dashed line is a simple average of the values between 10 and 14, and agrees well with the saturated value of the "Ostrach curve".

4. EXPERIMENTAL TEST RIG - "NACOSPANS"

To allow the study of systems of the proposed size for the SINQ target, a large scale test rig (again using water) has been built.This is shown in Fig. 15. The principle of this rig is similar to that for the small scale apparatus used for the flow visualisation. A glass cylinder of 20 cm diameter and 250 cm height is set in a square aquarium of 45 cm side and 300 cm height. A 40 cm long heating rod is inserted from the bottom which has a distributed heat generation decreasing exponentially with a relaxation length of 30 cm. This gives a first approximation to the expected beam heating.

The main purpose of this test rig is to measure temperature distributions. A total of 70 thermocouples are installed: on the heater surface, cylinder surface, bottom plate and inside the water. A glass tube of 16.2 cm diameter and 200 cm length is also available, to be used for experiments including a guide tube.

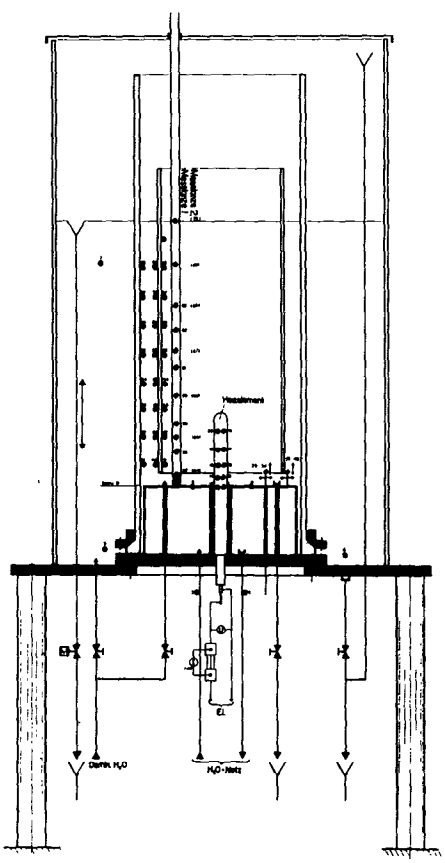

Fig. 15 Schematics of the large scale test rig (NACOSPANS).

Fig. 16 shows photographs of a general view of the test rig together with a part of the data taking system. The test rig is now in operation and experiments are in progress.

Fig. 16 Photograph of general view of the apparatus, NACOSPANS.

REFERENCES

1. Y. Takeda, Proceedings ICANS-VI, ANL (1982)
2. C. Tschalär, Proceedings ICANS-V, Jülich
3. S. Ostrach, Lecture note at Haifa Univ., Israel, 1978
4. E.R.G. Eckert, Int.J.Heat Mass Transfer, Vol. 2 (1961) 106